NANO LETTERS

pubs.acs.org/NanoLett

Mini-Review

Spatial Resolution in Nanoscale TERS Imaging: Current Status, Challenges, and Guidelines

Renato Zenobi,* Naresh Kumar,* and Prabhat Verma*

Cite This: *Nano Lett.* 2025, 25, 3707−3716

Read Online

ACCESS | Metrics & More | Article Recommendations

ABSTRACT: Tip-enhanced Raman spectroscopy (TERS) was invented almost 25 years ago and was quickly recognized as one of the few nano-optical techniques that confine light at the nanoscale to explore light−matter interactions at the nanoscale. Even several years after its invention, the spatial resolution in TERS studies is not only somewhat controversial, especially for AFM-based TERS measurements of samples at room temperature, but also not reported in the literature in a consistent, generally accepted fashion. This Mini-Review discusses the current situation and how spatial resolution in TERS is reported in different ways that yield different values because no standard method is defined. More importantly, the spatial resolution in TERS is influenced by various experimental conditions and other factors in a comprehensive fashion, which have often been ignored. We consider all possible factors that affect spatial resolution in TERS and provide guidelines on how to determine and report spatial resolution.

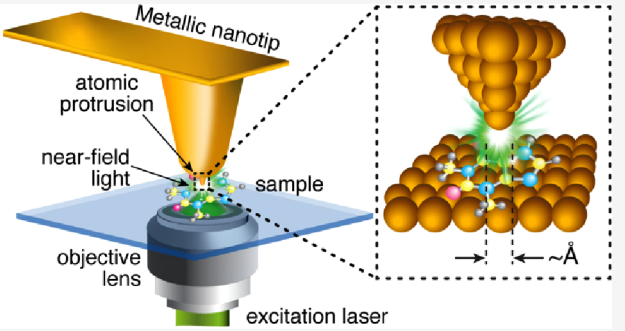

KEYWORDS: *Nanospectroscopy, nanoimaging, optical nanoconfinement, plasmonic enhancement, nanodrift*

1. INTRODUCTION

Tip-enhanced Raman spectroscopy (TERS), which combines the chemical specificity of Raman spectroscopy with the spatial resolution of scanning probe microscopy (SPM), such as AFM or STM, and the spatial confinement of light field, has been well-established and well-accepted as a nano-optical technique for nanoinvestigation and nanoimaging of a variety of samples. TERS, along with some other plasmonics-based techniques such as near-field luminescence imaging, is one of the very few apertureless optical techniques that physically confines light in a nanometric volume, making it possible to study the light−matter interaction at the nanoscale, enabling nanoscale mapping of various chemical, physical, and biological properties of a sample. Two important parameters for obtaining high-quality nanoimaging of a sample in TERS are the enhancement and confinement of the light field at the apex of the probe tip, both of which depend strongly on the experimental parameters, configurations, and environment and have received extensive attention in TERS research.[1,2] However, spatial resolution in TERS studies is often reported inconsistently, with various criteria employed by researchers to quantify it. Several metrics are commonly used: (i) The full width at half maximum (fwhm) of an isolated nanoscale feature in a TERS image is frequently taken as the measure of spatial resolution.[3] (ii) In some cases, the half width at half maximum (hwhm) is used, which effectively results in a resolution value that is better by a factor of 2.[4] (iii) Another method involves using the sharpest possible step edge in a TERS image, with resolution defined according to a 10%−90% criterion.[5] (iv) Occasionally, the resolution is simply equated to the pixel size used during data acquisition. Resolution may be determined from line scans or directly from TERS images,[6] and there is no universally accepted method for defining, determining, and reporting spatial resolution in TERS.

It is noteworthy that the spatial resolution reported in the literature for TERS varies widely, as detailed in Table 1.[3,4,7−17] Table 1 is *not* intended to present an exhaustive list of every TERS publication that reported a spatial resolution but rather a selection of key papers from the literature, including some resolution records and, possibly, exaggerations. The resolutions quoted in the selected examples range from approximately 0.15 nm to over 20 nm—an astonishing variation spanning more than 2 orders of magnitude. The reasons for this disparity are not entirely clear, though it likely stems from differences in the experimental conditions under which the TERS data were acquired. For instance, STM-TERS conducted under cryogenic conditions in ultrahigh vacuum (UHV) consistently achieves the best spatial resolution.[3,15,16] In contrast, ambient TERS,

Received: December 8, 2024
Revised: February 18, 2025
Accepted: February 21, 2025
Published: February 27, 2025

https://doi.org/10.1021/acs.nanolett.4c06273
Nano Lett. 2025, 25, 3707−3716

Table 1. Examples of Spatial Resolution Reported in TERS Studies Conducted at Ambient Conditions and under UHV/Cryogenic Conditions, in Chronological Order

Reference	Sample	Spatial resolution claimed	Step size	Imaging	AFM/STM-TERS	Environmental conditions	Drift reported?
			Ambient Conditions				
Kurouski et al., 2012[7]	Insulin fibril	**~1 nm**	1 nm	no	AFM	atmos, RT	no
Chen et al., 2014[4]	CNTs	**1.7 nm**[a]	0.6 nm	yes	STM	atmos, RT	1−2 nm/min
Lin et al., 2016[8]	ssDNA	**<1 nm**	0.3 nm	no	AFM	atmos, RT	0.5 nm/min
He et al., 2019[9]	ssDNA	**0.5 nm**	0.5 nm	(yes)[b]	AFM	atmos, RT	no
Cai et al., 2021[10]	CoTPP	**~2 nm**	2 nm	yes	STM	atmos, RT	<0.3 nm/s
Huang et al., 2020[11]	4-MBA	**<5 nm**	4−5 nm	no	STM	EC-TERS	no
Mrđenović et al., 2022[12]	Cell membrane	**20.3 ± 7.8 nm**	20 nm	yes	AFM	atmos, RT	
		2.5 ± 2.3 nm	1.5 nm	no			2.8 ± 2.3 nm/min
			UHV/Cryogenic Conditions				
Zhang et al., 2013[13]	H_2TBPP	**5 Å**	1.6 Å	yes	STM	80 K, UHV	1−5 Å/min
Liao et al., 2016[14]	CNTs	**7 Å**	2.5 Å	yes	STM	79 K, UHV	0.25 Å/min
Chiang et al., 2016[15]	H_2TBPP	**2.6 Å**	2.5 Å	no	STM	RT, UHV	no
Lee et al., 2019[3]	CoTPP	**1.67 ± 0.12 Å**	0.45 Å	yes	STM	6 K, UHV	no
Zhang et al., 2019[16]	Mg-porphine	**1.5 Å**	1 Å	yes	STM	~7 K, UHV	0.83 pm/min
Li et al. 2022[17]	borophene	**4.8 Å**	1.2 Å	yes	STM	78 K, UHV	1.5 Å/min

[a]Measured using half width at half maximum (hwhm). [b]Imaging was performed, but the DNA sample was pulled along the AFM scan direction; therefore, the TERS "image" was essentially reduced to a line profile.

often performed using AFM-TERS without a "gap mode" to confine the electromagnetic field beneath the tip, generally yields poorer resolution.[12,18] Factors such as system drift and the stability of atomic protrusions at the tip apex (sometimes referred to as "picotips") are also critical, and these issues will be discussed in detail in this Mini-Review. Additionally, the nature of the sample itself—such as a single-crystal surface versus the surface of a live cell in a culture medium—has a significant impact on the observed resolution. Nevertheless, some studies have reported remarkably good resolution, even for ambient TERS on biological samples.[12] One of our aims is thus to clarify whether such a good resolution is indeed achievable and, if so, under what specific conditions.

UHV/cryogenic TERS experiments with extremely flat samples, such as single crystal surfaces, provide a more controlled environment. Therefore, a discussion on the large discrepancies in spatial resolution should primarily focus on ambient TERS. A few research groups also conduct TERS in liquid environments, such as in electrochemical TERS studies.[19] The spatial resolution in these contexts is comparable to that in ambient TERS and will not be discussed separately. Readers are also referred to the review by Richard-Lacroix et al.,[20] which mostly attempted to justify the possibility of obtaining sub-nm-scale spatial resolution achievable under ambient conditions. In this Mini-Review, however, we take a broader approach to the issue of spatial resolution in TERS: our objective is to outline the factors that influence spatial resolution in TERS, critically evaluate the existing literature, and, building on previous studies that have touched on some of these issues,[1,21] provide a set of guidelines for accurately measuring and reporting spatial resolution.

2. FACTORS THAT INFLUENCE SPATIAL RESOLUTION

2.1. Step Size and Nyquist Criterion. In microscopy, the Nyquist−Shannon sampling theorem establishes a fundamental physical constraint on resolution, stating that the optimal resolution cannot be better than approximately 2.3 times the sampling frequency.[22,23] In the context of digital imaging, the sampling frequency is equivalent to the pixel size, and this principle applies universally across imaging techniques, including MRI, confocal microscopy, and scanning probe microscopy. For example, it has been demonstrated that even the apparent height of two-dimensional (2D) crystals imaged by AFM is influenced by the pixel size, as a pixel size that is too large will fail to accurately capture the highest protrusions of a 2D crystal.[24] Consequently, a basic requirement for reporting spatial resolution in scanning probe microscopy techniques such as TERS should be that it is no better than 2.3 times the pixel size used.

This approach contrasts with instances where researchers equate pixel size with the resolution, a practice that, at first sight, appears fundamentally flawed. The validity of this approach, however, depends on the size of the features on the sample surface that are being resolved. Consider Figure 1: The Nyquist criterion is applicable when the features are larger than the step or pixel size used (Case A). However, when the features on the sample surface are similar to (Case B) or smaller than (Case C) the pixel size, these features may appear in one pixel but not in the adjacent one (Figure 1). In such cases, it is reasonable to equate the spatial resolution with the pixel or step size. In this case, the pixel size/step size may be regarded as an upper bound to quote the experimental resolution, because the TERS tip itself may afford a better resolution.

The challenge, of course, is that one cannot, a priori, know how small features on a sample will be. Additionally, rapidly changing spectral signatures may be mistaken for resolvable features, although in reality they could be artifacts—originating from degradation products, or from contaminants that adhere to the TERS tip or appear transitorily on the sample surface (see Section 2.5).

As an obvious solution to this issue, we recommend imaging the area of interest more than once. If a small feature repeatedly appears in one pixel but not in adjacent pixels (allowing for some drift; see Section 2.2), then the resolution can be considered equivalent to the pixel size used. Reducing the pixel size could further sharpen the localization of such a small feature.

https://doi.org/10.1021/acs.nanolett.4c06273
Nano Lett. 2025, 25, 3707−3716

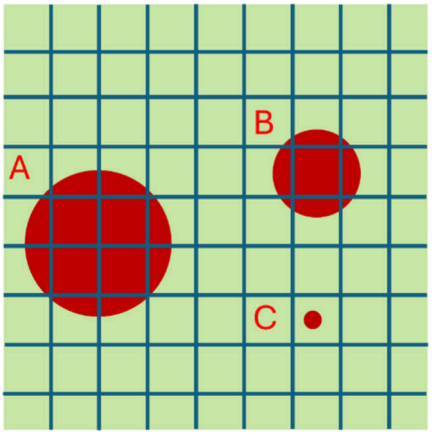

Figure 1. Sampling rate versus spatial frequency. When the step size (represented by the blue grid) in hyperspectral TERS imaging is smaller than the spatial frequency of the features in the sample, as illustrated by feature A, the Nyquist resolution criterion is applicable. However, if the step size is comparable to or significantly larger than the feature size, as exemplified by features B and C, respectively, the TERS signal will be confined to a single pixel. In such cases, the spatial resolution of the TERS image is effectively determined by the step size of the imaging grid.

Therefore, repeated and reproducible TERS imaging is crucial. A corollary is that the laser power must be kept low enough to avoid thermally degrading or displacing molecular features on the sample surface, which could result in their disappearance in subsequent scans.

2.2. Drift. A common question often posed is: why not simply increase the spatial resolution in TERS imaging under ambient conditions by reducing the step size? The answer to this question involves addressing the often overlooked yet crucial issue of drift. Drift is rarely quantified and reported in TERS studies. It hinders the continuous improvement of TERS resolution by limiting the effectiveness of reducing the step size during imaging, especially in 2D TERS imaging compared to line scans. Drift may originate either from molecular movement (molecular drift) or from the instrument itself (instrumental drift). Differentiating between these two sources of drift is challenging. Molecular drift may be exacerbated during laser illumination, although laser powers are typically kept low and heating is minimal. Nevertheless, this warrants further investigation: to the best of our knowledge, no studies have yet reported a direct comparison of drift with and without laser illumination. This section will address the phenomenon of drift in a general context and examine its implications for spatial resolution in TERS imaging.

While sample drift remains a considerable challenge at ambient conditions, it is significantly reduced when TERS measurements are conducted under UHV and cryogenic temperatures. For instance, in 2013, Dong's group reported a breakthrough by achieving UHV-TERS imaging of a single porphyrin molecule at 80 K with sub-nm spatial resolution.[13] In this study, the total imaging duration was only 2.7 min, and the thermal drift was reported to be 1.5 Å/min at 80 K. In another study, the same group reported a thermal drift of 1.5 nm/h (0.25 Å/min) at 79 K.[14] By 2019, Dong's group further improved the UHV-TERS spatial resolution to 1.5 Å by imaging a single Mg-porphine molecule at 7 K, reducing drift by more than 30-fold to below 0.83 pm/min.[16] In the same year, Apkarian's group reported UHV-TERS imaging of a Co-porphyrin molecule at 6 K with a spatial resolution of 1.67 Å, but with an imaging time of 2.3 h, indicating a considerably low drift of below 0.01 Å/min.[3] More recently, Jiang's group achieved UHV-TERS imaging of borophene at 78 K with a spatial resolution of 4.8 Å, where the drift was reported to be 1.5 Å/min.[17] These TERS studies in controlled UHV and cryogenic environments demonstrate the critical role of drift in determining spatial resolution. As the temperature is reduced from 78−80 K to 6−7 K, presumably the significant decrease in instrument and molecular drift extends the TERS spatial resolution to the angstrom scale.

While the UHV-TERS studies conducted under cryogenic conditions by the Dong, Apkarian, and Jiang groups demonstrated minimal drift, which enabled sub-molecular spatial resolution, the situation under ambient conditions is markedly different and more complex due to the nature of the samples studied. Recently, the Zenobi group measured drift in their bottom-illumination AFM-TERS system, which was based on a Bruker AFM, under ambient conditions.[12] This was achieved by recording time-lapse AFM images of single-wall carbon nanotubes (SWCNTs) on an atomically flat mica substrate. The first and the last frames of the 14 time-lapse AFM images, shown in Figures 2a and 2b, respectively, reveal a significant drift over time. A histogram of the drift, generated by analyzing consecutive AFM images, is presented in Figure 2c, indicating that the drift ranged from 0.5 to 6.0 nm/min, although occasionally it was as high as >19.0 nm/min. After excluding these outliers, the average drift was estimated at 2.8 ± 2.3 nm/min, a factor of 3−6 higher than the drift reported in previous TERS studies by Lin et al. (0.5 nm/min)[8] and Chen et al. (1−2 nm/min).[4] A drift of the order of 1−2 nm/min at room temperature appears typical, and it will probably be worse for systems where diffusion or movement can occur, or for older scanning piezo elements.

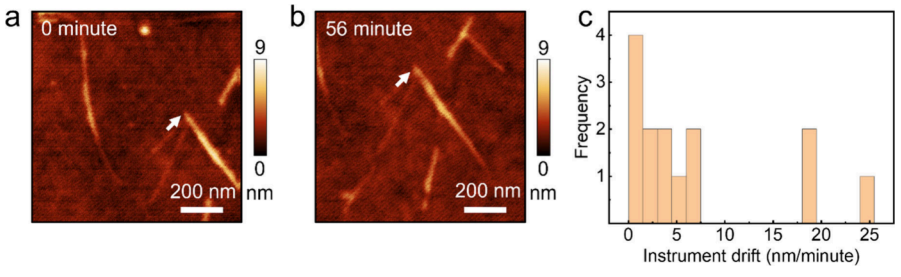

Figure 2. AFM topography images of SWCNTs on mica substrate recorded at (a) 0 and (b) 56 min in tapping mode. The measurement time of each AFM image was 4 min. (c) Histogram of the drift (nm/min) estimated by analyzing 14 time-lapse AFM images of the SWCNTs. Adapted with permission from ref 12. Copyright 2022, Wiley-VCH GmbH.

https://doi.org/10.1021/acs.nanolett.4c06273
Nano Lett. 2025, 25, 3707−3716

An obvious question that arises from the drift analysis is, Can drift be minimized or compensated under ambient conditions, without lowering the temperature? This was addressed in a recent study by the Verma group,[25] where significant advancements were made to minimize drift along the optical axis (z-direction). A real-time focus stabilization system was developed using a piezo-controlled objective scanner combined with laser reflection-based positional sensing. This system could maintain the focal plane within ±5 nm over 8 h, effectively eliminating focus drift and ensuring the stability of the TERS signal during long-duration measurements. For lateral drift (x−y directions), the study employed a laser-scanning-assisted technique. Galvanometer mirrors were used to rapidly raster scan the laser spot around the metallic tip, generating a Rayleigh scattering image that identified the tip's position. Using a feedback system, the relative position of the tip and laser focus was corrected automatically, achieving lateral drift compensation within ±10 nm over 1.5 h. This enhanced stability allowed these researchers to capture high-resolution images of large-sized WS_2 layers over a 6-h period (12× longer than the conventional imaging durations) without significant signal degradation, enabling the detection of rare defect-related signals.

While drift compensation is not available in every laboratory, we strongly recommend measuring and reporting the drift of the TERS system along with the spatial resolution.

2.3. Tip Type, Size, and Geometry. Two types of tips are generally used in TERS, metal-coated dielectric tips and solid metallic tips. While the metal-coated tips, which are often made by evaporating or sputtering metal on the shaft of an AFM tip, are frequently used in contact-mode or tapping-mode AFM-TERS, the solid metallic tips, which are usually made by electrochemical etching of metal nanowires, are commonly used in STM-TERS and shear-force-mode AFM-TERS. The dominating mechanisms for field confinement and enhancement in these two types of tips are different. While the process of localized surface plasmon resonance (LSPR) dominates the confinement and enhancement of light in metal-coated tips, the lightning rod effect dominates in stand-alone solid metallic tips. It is generally accepted that the spatial resolution in TERS is comparable to the size of the tip apex for both types of tips. However, recent publications have demonstrated surprisingly good spatial resolution that is considerably better than the size of the tip apex. In most cases, the authors explain this with the existence of atomic protrusions at the tip apex, so that the resolution can still be compared with the size of the extreme apex, ultimately a single metal atom.[26]

In the case of metal-coated tips, a thin and rough metallic layer is evaporated on the tip body, which is equivalent to depositing multiple metal nanoparticles. These nanoparticles behave like optical antennas, and their size as well as the interparticle gaps determine which wavelength will be best enhanced through plasmon resonance and how tightly it will be confined.[27] To create a reasonably strong plasmon resonance for a target wavelength, the antennas should have a specific size, somewhere around one-tenth to one-fifth of the wavelength, which originally was thought to limit the spatial resolution in TERS. A much smaller metal particle would not provide high enhancement due to the lack of strong plasmon resonance, making it practically challenging to observe Raman scattering from a sample, particularly a weakly scattering sample. Consequently, the commonly reported tip apex size was about 20−50 nm, which produced a spatial resolution of about 20−30 nm in the past.[28] With the advancement of instrumentation and experimental skills, it is now commonly reported that a metal-coated tip can produce a spatial resolution of about 10 nm or less under ambient conditions.[6,29]

On the other hand, the surface of a solid metallic tip fabricated by the electrochemical etching method is relatively smooth, with no metal nanoparticles on the body, making it unsuitable for producing plasmon resonance in the visible range. Consequently, the lightning rod effect becomes the dominating mechanism for the confinement and enhancement of light for a solid metallic tip. Here also, light confinement depends on the apex size but is largely wavelength-independent. The typical apex size for electrochemically etched solid metallic tips was reported to be about 20−70 nm in the past, and accordingly, the spatial resolution in TERS utilizing solid metallic tips was also reported to be about 20−30 nm,[30] the same as in the case of metal-coated tips. Once again, with improved instrumentation and experimental skills, a spatial resolution with solid metallic tips, even under ambient conditions, is now frequently reported to be about 10 nm or less.[31,32]

Since the lightning rod effect is a nonresonant phenomenon, a solid metallic tip with a very sharp apex is expected to provide much tighter confinement without a strong influence of the apex size, and hence, much better spatial resolution in TERS could be obtained. Although it is practically very challenging to deliberately fabricate a solid metallic tip with an extremely small apex, obtaining a tip with a single metal atom protruding at the apex is apparently still possible by chance or with some special skill, such as by contacting the tip with a metal surface under a controlled environment and pulling out a few atoms that can stick to the tip apex. Figures 3a and 3b illustrate a comparison between a smooth solid metallic tip and a similar tip with a tiny protrusion at the apex. For such tips, which we will refer to as "tips with an atomic protrusion", achieving sub-nanometric or even sub-atomic spatial resolution ought to be possible because the lightning rod effect can confine the light at the protruding atom. Similarly, it might also be possible to obtain a tiny metallic protrusion at the apex of a metal-coated tip (Figure 3c). The metal-coated tip can have suitably sized metal nanoparticles deposited on the body, including at the apex, for

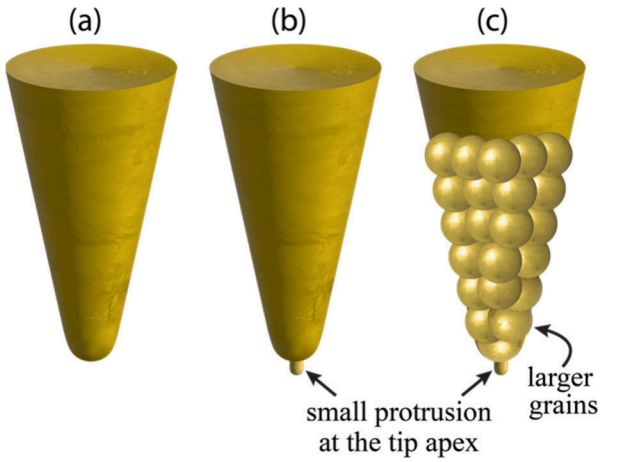

Figure 3. Illustrations of TERS tips: (a) a smooth solid metal tip, (b) a smooth solid metal tip with an atomic protrusion at the apex, and (c) a metal-coated tip with a tiny metallic protrusion at the apex. While the larger grains on the tip body in (c) can plasmonically enhance the light field, the atomic protrusion at the apex can highly localize this enhanced field near the protrusion.

https://doi.org/10.1021/acs.nanolett.4c06273
Nano Lett. 2025, 25, 3707−3716

good plasmon resonance, and a very small nanoparticle right below the apex, where the plasmonically enhanced field around the larger particle at the apex can be channeled down through the small particle below the apex to provide a tight confinement of the light field. Therefore, one can expect to achieve an angstrom-level or even better spatial resolution for both types of tips if an atomic protrusion can be created and sustained at the apex.

A major concern, however, is about the longevity of such a protrusion, which can easily drift away from the tip apex or be destroyed either by the environment or during the experimental process, as it is expected to be only weakly attached to the tip. Particularly under ambient conditions, such protrusions will not survive long, while they have a better chance of survival at cryogenic temperatures in UHV. Several researchers have been recently able to fabricate such an STM tip with an atomic protrusion inside the UHV system and demonstrate that the atomic protrusion can survive the entire measurement period. When these tips are used in the gap-mode configuration, which is an essential part of STM-TERS measurement where the sample molecules are sandwiched between the tip apex and a metal substrate, the enhancement increases by about 100×.[33] In addition to the lightning rod effect, the gap-mode configuration also allows the plasmonic effects to become significant for a resonant illumination, as one can consider the interaction of a localized dipole at the tip apex and its image in the metal substrate to activate the gap-mode plasmon resonance.[33] All these factors favor measuring extremely weak Raman signals from the sample area under the atomic protrusion at the tip apex. This has recently allowed several researchers to observe atomic- and sub-atomic-level spatial resolution in STM-TERS.[3,13,34] It must, however, be noted that extraordinarily good spatial resolution was almost always obtained under very strict experimental conditions of gap-mode configuration, resonant illumination, UHV, and cryogenic temperatures. While gap-mode geometry and illumination with a wavelength that resonates with the gap-mode plasmons can significantly improve the enhancement, UHV and low temperatures can effectively protect the tip and the sample from atmospheric contamination and minimize drift to picometer scale, which helps in measuring a weak scattering sample with high spatial resolution. UHV also reduces photobleaching and improves the signal-to-noise ratio, which further helps in TERS measurement with improved spatial resolution.

Atomic-level resolution has not yet been demonstrated under ambient conditions, either with a metal-coated tip or with a solid metallic tip. Environmental factors (e.g., the presence of oxygen that can oxidize the sample molecules and some metals, carbon and sulfur contaminants that can contaminate the tip and deteriorate the field enhancement, other atmospheric molecules that can diffuse onto the sample, humidity that can create a water layer on the sample) prevent practical observation of weak Raman signals under ambient conditions. Furthermore, not only do chemical interactions of the atmospheric contaminants with the tip and the sample molecules escalate at room temperature, but also drift, diffusion, rotation, and other fluctuations of the sample molecule increase. Most importantly, at ambient conditions and room temperature, atomic protrusions at the apex, if obtained, will not be stable. Even though theoretical considerations suggest that atomic-scale spatial resolution could be achievable, observing atomic-level resolution in ambiance is practically extremely challenging.

Some recent reports have suggested that a resolution in the low nm range under ambient conditions is possible with certain restrictions. For example, a 3 nm resolution was reported with a solid metallic tip in STM-TERS, which was estimated from the scanning step size,[34] and a 2.5 nm resolution was reported for a metal-coated tip in AFM-TERS of cell surfaces,[12] where it was noted that such high-resolution data was only possible if the measurement time was drastically reduced to counteract drift by performing line scans. Lin et al. claimed a resolution of 1 nm with a metal-coated tip in a gap-mode AFM-TERS under ambient conditions[8] by measuring TERS signals from a single-stranded DNA. Although the authors used a scan step of 0.5 nm and estimated a spatial resolution of about 1 nm from the variation in the Raman spectra, a TERS image was not provided. This shows that achieving true nanometer spatial resolution in TERS under ambient conditions is still a challenge, and it has been claimed only with certain restrictions, such as for a short measurement time or without a clear TERS image. There are no reports available on atomic-level spatial resolution under ambient conditions.

2.4. TERS Enhancement. As also indicated in Section 2.3, another critical factor that directly influences spatial resolution in TERS is the enhancement factor of the metallic TERS tips. This is particularly important for non-gap-mode AFM-TERS measurements (without a metallic substrate), where plasmonic signal enhancement is significantly lower and the far-field background is considerably higher compared to the gap-mode TERS measurements (with a metallic substrate). Two key parameters are typically used to evaluate the enhancement provided by a TERS tip: contrast and the enhancement factor. Contrast is defined as the ratio of the near-field signal intensity to the far-field signal intensity. The enhancement factor, however, provides a more comprehensive measure by accounting for the difference in the spatial extent of the near-field and far-field signal sources. Specifically, the enhancement factor is calculated by multiplying the contrast by the ratio of the far-field to near-field volumes. For thin-film and monolayer samples, the corresponding surface areas can be used in place of volumes to determine the enhancement factor:[2]

$$EF = \frac{I_{NF}}{I_{FF}}\frac{A_{FF}}{A_{NF}} = C\frac{A_{FF}}{A_{NF}} \quad (1)$$

where I_{NF} and I_{FF} are the Raman peak intensities measured in the near-field and far-field, respectively, A_{NF} and A_{FF} are the near-field and far-field probe areas, respectively, and C is the contrast. Here I_{NF} represents the Raman intensity of pure near-field, which is determined by subtracting the far-field Raman intensity (tip-out) from the measured TERS intensity (tip-in). Given the challenges in accurately determining the probe areas associated with TERS near-field and far-field regions, contrast serves as a more practical metric for assessing the enhancement capability of a TERS probe. High contrast is achieved under resonance when the localized surface plasmon frequency (ν_{LSP}) of the tip apex in the case of AFM-TERS or a gap-mode resonance in the case of STM-TERS matches the frequency of the excitation laser (ν_{Laser}).[35−37] A high contrast indicates a strong enhancement of Raman signals, leading to a high signal-to-noise ratio in the TERS spectrum. Strong Raman signals enable shorter acquisition times during TERS imaging, significantly reducing the overall imaging duration and, at the same time, providing higher contrast. Consequently, pixels with smaller step sizes can be used during hyperspectral TERS imaging, ultimately

https://doi.org/10.1021/acs.nanolett.4c06273
Nano Lett. 2025, 25, 3707−3716

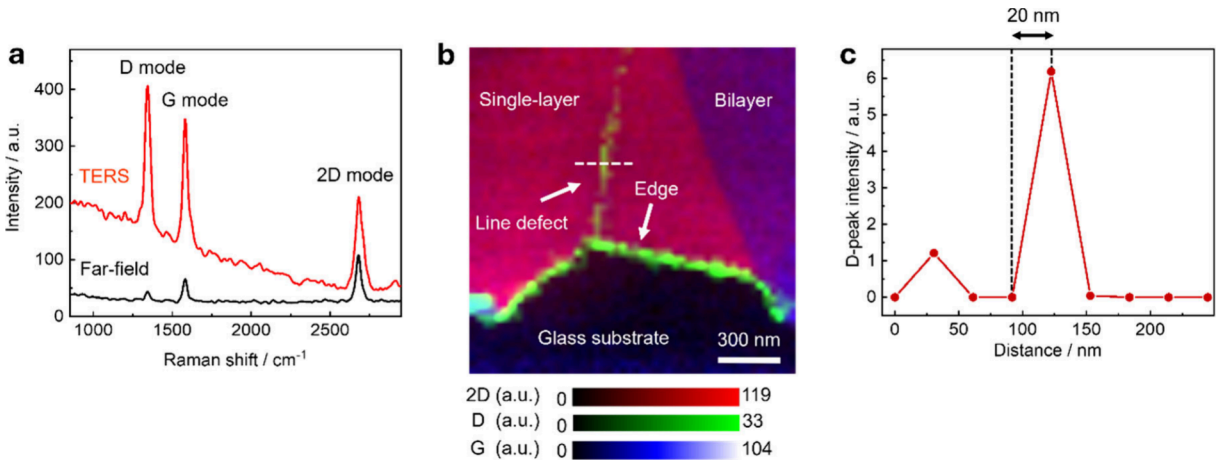

Figure 4. (a) TERS and far-field spectra measured from a single-layer graphene on a glass substrate in non-gap-mode geometry. (b) Overlay of the TERS images' D-mode, G-mode, and 2D-mode signals measured using TERS. Step size: 20 nm. (c) D-mode intensity profile across the dashed line marked in panel b. D-mode signal is observed in a single pixel, indicating that the width of the structural defect in the single-layer graphene sheet is smaller than the step size of the TERS image (Figure 1). Notably, this line defect was undetectable in both far-field Raman and AFM topography images. Panel b is adapted and panels a and c are redrawn with permission from ref 38. Copyright 2016, Royal Society of Chemistry.

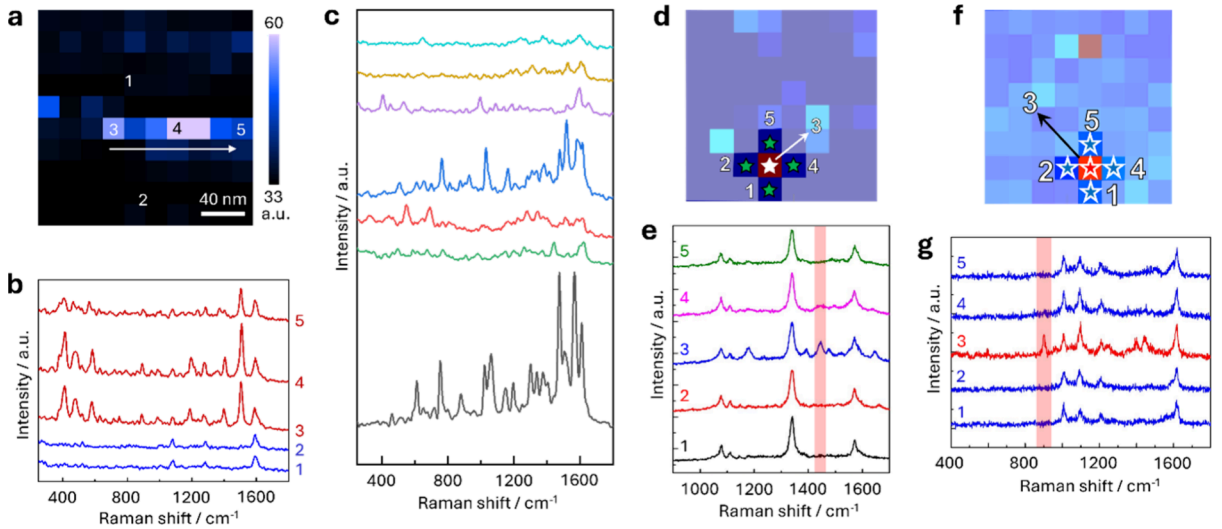

Figure 5. (a) TERS map of a biphenyl thiol (BPT)-functionalized Au(111) surface acquired using full-spectrum intensity. Step size: 20 nm. A pronounced high-intensity signal is observed along a straight line in the center of the image. (b) TERS spectra collected at positions 1−5, as indicated in panel a. The spectra at positions 1 and 2 exhibit the characteristic Raman signatures of BPT. In contrast, the spectra obtained along the central line (positions 3−5) differ markedly from the typical BPT spectrum, which can be attributed to atmospheric contaminants adhering to the TERS tip and being subsequently dragged across the surface before being discarded. (c) Raman spectra recorded from the apex of a freshly prepared silver-coated tip in an ambient environment without contacting the sample. The time-dependent spectra reveal significant variations in intensity and relative peak positions, indicative of SERS activity arising from the granular silver coating near the tip apex. (d) TERS map showing the *p,p′*-dimercaptoazobenzene (DMAB) signal intensity on a 4-nitrothiophenol (4-NTP)-functionalized Au(111) surface, with a step size of 3.3 nm. (e) TERS spectra corresponding to the pixels labeled 1−5 in panel d. Notably, only pixel 3 displays the characteristic DMAB signal, while the surrounding pixels exhibit the characteristic 4-NTP signal, indicating a spatial resolution of 3.3 nm. (f) TERS map of the 890 cm^{-1} signal obtained from a pyridine-4-thiol (4-PyS)-functionalized Au(111) surface, with a step size of 5 nm. (g) TERS spectra recorded at the pixels labeled 1−5 in panel f. While the spectra from pixels 1, 2, 4, and 5 display the characteristic peaks of 4-PySH, the spectrum from pixel 3 exhibits additional bands. Based on supporting DFT calculations, the TERS spectrum at pixel 3 was attributed to the 4-PyS-SH intermediate species. Panels a−c show unpublished data. Panels d and e are adapted with permission from ref 32. Copyright 2022, American Chemical Society. Panels f and g are adapted with permission from ref 47. Copyright 2022, American Chemical Society.

improving the spatial resolution of the acquired TERS image in accordance with the Nyquist criterion.

For instance, using non-gap-mode TERS in a bottom illumination geometry, Su et al. achieved a contrast of 15.8 for the D-mode Raman intensity measured from a single-layer graphene on a glass substrate, as shown in Figure 4a.[38] The high contrast of TERS signals enabled imaging a single-layer graphene sample with a spatial resolution of 20 nm, as demonstrated in Figure 4b. This high spatial resolution allowed the detection of a line defect within the graphene sheet, which was undetectable in the far-field Raman and AFM topography images. It should be noted that this analysis does not account for the local (D-mode) and nonlocal (G-mode and 2D-mode) nature of Raman signals in single-layer graphene, which are also important factors in the context of TERS measurements.[39]

https://doi.org/10.1021/acs.nanolett.4c06273
Nano Lett. 2025, 25, 3707−3716

A high TERS contrast and therefore a high spatial resolution are closely linked to tuning the ν_{LSP} of the tip or the gap resonance to the ν_{Laser} of the excitation laser. In the case of AFM-TERS, this alignment can be achieved through several approaches, including modifying the refractive index of the AFM tip before metallization,[40,41] adjusting the grain density of the metal coating,[28] and altering the size of the metal nanostructure at the tip apex.[42]

2.5. Single-Pixel Variability in TERS Spectra. In the TERS literature, it is frequently reported that line scans conducted under ambient conditions exhibit significant spectral variability, particularly when measured at intervals of just a few nanometers (and sometimes even <1 nm).[43,44] In these cases, TERS spectra can vary dramatically from one pixel to the next in terms of the number and relative intensities of peaks, often resulting in no two spectra within a TERS line scan being identical. Additionally, there are instances where a TERS signal is only observed at a single pixel, while the surrounding pixels of a 2D TERS map show entirely different spectra. Such pixel-to-pixel spectral differences are sometimes interpreted as evidence that the spatial resolution of the TERS line scan or image is equivalent to the pixel size. However, a critical question arises: How can we be certain that these spectral variations genuinely reflect the surface chemistry of the sample rather than being artifacts due to transient contamination of the tip or sample degradation?

In TERS imaging under ambient conditions, single-pixel variability in TERS spectra can arise from four different sources:

i. Tip Contamination. Contamination of the tip apex is a common source of spectral variability.[45] Tip contamination can occur due to the attachment of molecules either from the sample or from the ambient environment to the tip. This contamination often manifests itself as horizontal streaks across one or several lines in the TERS image, as the tip drags the picked-up molecules across the sample before eventually discarding them, as depicted in Figures 5a and 5b. In other instances, the entire TERS image may exhibit uniform signal intensity with minimal variation, suggesting possible tip contamination. To rule out this possibility, the cleanliness of the tip should be confirmed immediately after TERS imaging by measuring its spectrum on a clean substrate. It is important to note that simply measuring the "tip spectrum" in the absence of a substrate is inadequate, particularly in gap-mode TERS. For accurate assessment, the tip spectrum should be recorded on the same type of clean substrate (e.g., metal or glass) used for the sample.

ii. SERS Activity of the Tip Shaft. For metal-coated AFM-TERS tips, the granular morphology of the tip shaft, within a few hundred nanometers of the apex, can sometimes induce unintended surface-enhanced Raman scattering (SERS) activity. In such cases, atmospheric carbon contaminants may be captured in the SERS hotspots present on the tip shaft, causing rapid changes in the number and relative intensity of peaks, as shown in Figure 5c. In the SERS literature, this phenomenon is known as "blinking".[46] To rule out SERS activity from the tip shaft, time-dependent spectra should be measured by holding the tip stationary at a single location on the sample. Alternatively, time-dependent spectra can be acquired by placing the tip in contact with a clean substrate (similar to the one on which the analyte is placed). If rapid spectral variation is observed in these time-dependent measurements, it would suggest that the observed spectral changes are due to SERS activity from the tip.

iii. Sample Spectrum. In some instances, the TERS spectrum observed in a single pixel during imaging may perfectly match the expected spectrum of the sample, while the TERS spectra from surrounding pixels either exhibit no peaks or display peaks corresponding to a different molecule or compound, as demonstrated in Figures 5d and 5e.[47] Since spatial resolution is defined as the ability to distinguish the smallest features of a sample, if it is confirmed that only one pixel is showing the sample signal, the claim that the TERS resolution equals the pixel size can be justified. This is because features smaller than a single pixel have been successfully resolved in the TERS image (Figure 1).

iv. Spectrum of an Unusual Compound or Intermediate. If a TERS spectrum observed in a single pixel does not fully match the expected sample spectrum and exhibits no streaking or blinking behaviors, it could arise from an "intermediate" species involved in the surface chemical transformation under investigation, as shown in Figures 5f and 5g.[47] In this scenario, it is essential to document both the anomalous TERS spectrum detected at the single pixel and the TERS spectra observed in the adjacent pixels. Furthermore, to confidently assign the spectrum to an intermediate, density functional theory (DFT) calculations of potential intermediates should be performed and compared with the measured TERS spectrum. Only if a satisfactory match with the calculated spectrum is achieved should the spectrum be attributed to the corresponding intermediate. In such a case, the spatial resolution of the TERS image can be considered equal to the pixel size.

The factors discussed above emphasize that single-pixel variability in TERS spectra can originate either from the sample itself or from contamination. However, to accurately determine the source of this spectral variability, it is crucial to record locations with such single-pixel variations more than once, either with the same or a smaller step size, perform control measurements that verify the cleanliness of the tip, or perform supporting DFT calculations that confirm intermediate detection. Without these control measurements and calculations, the reliability of the TERS data cannot be assured, and any conclusions regarding the surface chemistry of the sample and the spatial resolution achieved would be questionable.

3. CONCLUSIONS AND GUIDELINES

Based on the concepts and discussion above, we give guidelines about how to best determine and report spatial resolution in TERS at the end of this text (below).

One frequently neglected issue is drift, which definitely needs to be considered. From the integration time per pixel (in s) and the drift (in nm/s), it can then be estimated whether drift will or will not influence the fidelity of the localization and, thereby, the spatial resolution. Drift can significantly impact spatial resolution and must be considered when reducing step size in imaging. To minimize drift during long-duration measurements under ambient conditions, it is recommended to utilize advanced stabilization techniques, such as real-time focus stabilization systems and lateral drift compensation methods, as demonstrated by Kato et al.[25]

To achieve high spatial resolution in TERS imaging, the enhancement factor of TERS tips should be maximized, which allows short acquisition times and imaging of the relevant areas without being too much affected by drift. This requires aligning the localized surface plasmon (ν_{LSP}) frequency of the TERS tip apex with the excitation laser frequency (ν_{Laser}).

https://doi.org/10.1021/acs.nanolett.4c06273
Nano Lett. 2025, 25, 3707−3716

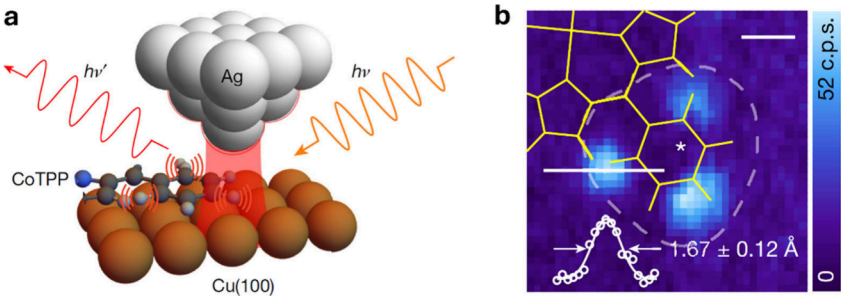

Figure 6. (a) Schematic diagram of the TERS setup to image a single Co-porphyrin molecule on a Cu(111) surface under UHV and cryogenic conditions. (b) Overlay of the molecular frame and TERS image of the 2986−2995 cm^{-1} spectral region (C−H stretching) showing the phenyl moiety of the Co-porphyrin molecule. Inset, intensity profile of TERS signal over one of the C−H bonds fitted with a Gaussian curve. The spatial resolution was determined from the fwhm of the Gaussian fit to be 1.67 ± 0.12 Å. Adapted with permission from ref 3. Copyright 2019, Springer Nature Publishing.

If possible, repeat measurements should also be performed by imaging the same sample area more than once—although we do acknowledge that, due to drift, repeat measurements of the exact same area may be challenging. Nevertheless, the consistent appearance of a spectral feature in the same pixel across multiple scans will support the validity of the observed resolution, suggesting that the variability reflects actual surface features rather than artifacts.

Figure 6 shows an example where the spatial resolution was properly determined and reported.[3] We note in particular that Figure 6b is an image, not just a line scan, the lobes of the molecule that are shown do not line up with the scan direction, and the fwhm of the TERS peak on the left was reported along a line that was put through it after TERS imaging.

The only "blind spot" in this paper is that the drift of the system was not reported; on the other hand, this was also the case for a few other recent TERS studies in UHV or at cryogenic temperatures that reported sub-molecular resolution (see Table 1).

The field of TERS currently lacks sufficient *quantitative* studies, such as those by Mrđenović et al.[12] and Kato et al.,[25] which systematically explore the factors that influence spatial resolution. Expanding on this aspect through rigorous quantitative investigations is imperative for advancing the understanding and capabilities of TERS, in particular with respect to spatial resolution. We therefore encourage the TERS community to prioritize such efforts, as they are essential for elucidating the factors that govern spatial resolution and for driving further innovation in nanoscale chemical imaging.

Recommendations on How to Accurately Measure and Report TERS Resolution.

- It is recommended to use the fwhm of the TERS signal from a very small feature on the sample surface to determine and quote the spatial resolution. In any case, the metric (10%−90%/fwhm/hwhm) used must be indicated.
- The drift of the system should be measured and reported in the TERS studies, especially when claiming exceptionally high spatial resolution under ambient conditions.
- Before and after TERS imaging, the SERS activity of the TERS tips should be checked, to rule out spectral changes (e.g., blinking) originating from contaminants. Obviously, tips that show such behavior should not be used for TERS imaging.
- When single-pixel variability is observed, it is recommended to reimage the same area at least one more time, if possible with a different (smaller) step size.

AUTHOR INFORMATION

Corresponding Authors

Renato Zenobi − *Department of Chemistry & Applied Biosciences, ETH Zurich, CH-8093 Zürich, Switzerland;* orcid.org/0000-0001-5211-4358; Email: zenobi@org.chem.ethz.ch

Naresh Kumar − *Department of Chemistry & Applied Biosciences, ETH Zurich, CH-8093 Zürich, Switzerland;* orcid.org/0000-0001-8953-5420; Email: naresh.kumar@org.chem.ethz.ch

Prabhat Verma − *Department of Applied Physics, Osaka University, Suita, Osaka 565-0871, Japan;* orcid.org/0000-0002-7781-418X; Email: verma@ap.eng.osaka-u.ac.jp

Complete contact information is available at: https://pubs.acs.org/10.1021/acs.nanolett.4c06273

Notes

The authors declare no competing financial interest.

REFERENCES

(1) Wang, X.; Huang, S.-C.; Huang, T.-X.; Su, H.-S.; Zhong, J.-H.; Zeng, Z.-C.; Li, M.-H.; Ren, B. Tip-Enhanced Raman Spectroscopy for Surfaces and Interfaces. *Chem. Soc. Rev.* **2017**, *46*, 4020.

(2) Kumar, N.; Mignuzzi, S.; Su, W.; Roy, D. Tip-Enhanced Raman Spectroscopy: Principles and Applications. *EPJ. Techn. Instrum.* **2015**, *2*, 1−23.

(3) Lee, J.; Crampton, K.; Tallarida, N.; Apkarian, V. A. Visualizing Vibrational Normal Modes of a Single Molecule with Atomically Confined Light. *Nature* **2019**, *568*, 78−82.

(4) Chen, C.; Hayazawa, N.; Kawata, S. A. 1.7 nm Resolution Chemical Analysis of Carbon Nanotubes by Tip-Enhanced Raman Imaging in the Ambient. *Nat. Commun.* **2014**, *5*, 3312.

(5) Shao, F.; Dai, W.; Zhang, Y.; Zhang, W.; Schlüter, A. D.; Zenobi, R. Chemical Mapping of Nanodefects within 2D Covalent Monolayers by Tip-Enhanced Raman Spectroscopy. *ACS Nano* **2018**, *12* (5), 5021−5029.

(6) Su, W.; Kumar, N.; Krayev, A.; Chaigneau, M. In Situ Topographical Chemical and Electrical Imaging of Carboxyl Graphene Oxide at the Nanoscale. *Nat. Commun.* **2018**, *9*, 2891.

(7) Kurouski, D.; Deckert-Gaudig, T.; Deckert, V.; Lednev, I. K. Structure and Composition of Insulin Fibril Surfaces Probed by TERS. *J. Am. Chem. Soc.* **2012**, *134*, 13323−13329.

(8) Lin, X.-M.; Deckert-Gaudig, T.; Singh, P.; Siegmann, M.; Kupfer, S.; Zhang, Z.; Gräfe, S.; Deckert, V. Direct Base-to-Base Transitions in ssDNA Revealed by Tip-Enhanced Raman Scattering. *arXiv Preprint* **2016**, DOI: 10.48550/arXiv.1604.06598.
(9) He, Z.; Han, Z.; Kizer, M.; Linhardt, R. J.; Wang, X.; Sinyukov, A. M.; Wang, J.; Deckert, V.; Sokolov, A. V.; Hu, J.; Scully, M. O. Tip-Enhanced Raman Imaging of Single-Stranded DNA with Single Base Resolution. *J. Am. Chem. Soc.* **2019**, *141*, 753−757.
(10) Cai, Z.-F.; Zheng, L.-Q.; Zhang, Y.; Zenobi, R. Molecular-Scale Chemical Imaging of the Orientation of an On-Surface Coordination Complex by Tip-Enhanced Raman Spectroscopy. *J. Am. Chem. Soc.* **2021**, *143*, 12380−12386.
(11) Huang, S.-C.; Wang, X.; Zhao, Q.-Q.; Zhu, J.-F.; Li, C.-W.; He, Y.-H.; Hu, S.; Sartin, M. M.; Yan, S.; Ren, B. Probing Nanoscale Spatial Distribution of Plasmonically Excited Hot Carriers. *Nat. Commun.* **2020**, *11*, 4211.
(12) Mrđenović, D.; Ge, W.; Kumar, N.; Zenobi, R. Nanoscale Chemical Imaging of Human Cell Membranes Using Tip-Enhanced Raman Spectroscopy. *Angew. Chem., Int. Ed.* **2022**, *61*, No. e202210288.
(13) Zhang, R.; Zhang, Y.; Dong, Z. C.; Jiang, S.; Zhang, C.; Chen, L. G.; Zhang, L.; Liao, Y.; Aizpurua, J.; Luo, Y.; Yang, J. L.; Hou, J. G. Chemical Mapping of a Single Molecule by Plasmon-Enhanced Raman Scattering. *Nature* **2013**, *498*, 82−86.
(14) Liao, M.; Jiang, S.; Hu, C.; Zhang, R.; Kuang, Y.; Zhu, J.; Zhang, Y.; Dong, Z.-C. Tip-Enhanced Raman Spectroscopic Imaging of Individual Carbon Nanotubes with Subnanometer Resolution. *Nano Lett.* **2016**, *16*, 4040−4046.
(15) Chiang, N.; Chen, X.; Goubert, G.; Chulhai, D. V.; Chen, X.; Pozzi, E. A.; Jiang, N.; Hersam, M. C.; Seideman, T.; Jensen, L.; Van Duyne, R. P. Conformational Contrast of Surface-Mediated Molecular Switches Yields Ångstrom-Scale Spatial Resolution in Ultrahigh Vacuum Tip-Enhanced Raman Spectroscopy. *Nano Lett.* **2016**, *16*, 7774−7778.
(16) Zhang, Y.; Yang, C.; Ghafoor, A.; Zhang, Y.; Zhang, Y.-F.; Wang, R.-P.; Yang, J.-L.; Luo, Y.; Dong, Z.-C.; Hou, J. G. Visually Constructing the Chemical Structure of a Single Molecule by Scanning Raman Picoscopy. *Nat. Sci. Rev.* **2019**, *6*, 1169−1175.
(17) Li, L.; Schultz, J. F.; Mahapatra, S.; Lu, Z.; Zhang, X.; Jiang, N. Chemically Identifying Single Adatoms with Single-Bond Sensitivity During Oxidation Reactions of Borophene. *Nat. Commun.* **2022**, *13*, 1796.
(18) Gadelha, A. C.; Ohlberg, D. A. A.; Rabelo, C.; Neto, E. G. S.; Vasconcelos, T. L.; Campos, J. L.; Lemos, J. S.; Ornelas, V.; Miranda, D.; Nadas, R.; Santana, F. C.; Watanabe, K.; Taniguchi, T.; van Troeye, B.; Lamparski, M.; Meunier, V.; Nguyen, V.-H.; Paszko, D.; Charlier, J.-C.; Campos, L. C.; Cancado, L. G.; Medeiros-Ribeiro, G.; Jorio, A. Localization of Lattice Dynamics in Low-Angle Twisted Bilayer Graphene. *Nature* **2021**, *590*, 405−410.
(19) Huang, T.-X.; Cong, X.; Wu, S.-S.; Wu, J. B.; Bao, Y. F.; Cao, M. F.; Wu, L.; Lin, M. L.; Wang, X.; Tan, P. H.; Ren, B. Visualizing the Structural Evolution of Individual Active Sites in MoS_2 During Electrocatalytic Hydrogen Evolution Reaction. *Nat. Catal.* **2024**, *7*, 646−654.
(20) Richard-Lacroix, M.; Zhang, Y.; Dong, Z.-C.; Deckert, V. Mastering High Resolution Tip-Enhanced Raman Spectroscopy: Towards a Shift of Perception. *Chem. Soc. Rev.* **2017**, *46*, 3922−3944.
(21) Deckert, V.; Deckert-Gaudig, T.; Diegel, M.; Gotz, I.; Langeluddecke, L.; Schneidewind, H.; Sharma, G.; Singh, P.; Singh, P.; Trautmann, S.; Zeisberger, M.; Zhang, Z. Spatial Resolution in Raman Spectroscopy. *Faraday Discuss.* **2015**, *177*, 9−20.
(22) Shannon, C. E. Communication in the Presence of Noise. *In Proceedings of the IRE* **1949**, *37*, 10−21.
(23) Price, R. L., Jerome, W. G., Eds. *Basic Confocal Microscopy*, 1st ed.; Springer: New York, 2011. DOI: 10.1007/978-0-387-78175-4.
(24) Heymann, J. B.; Möller, C.; Müller, D. J. Sampling Effects Influence Heights Measured with Atomic Force Microscopy. *J. Microsc.* **2002**, *207*, 43−51.
(25) Kato, R.; Moriyama, T.; Umakoshi, T.; Yano, T.; Verma, P. Ultrastable Tip-Enhanced Hyperspectral Optical Nanoimaging for Defect Analysis of Large-Sized WS_2 Layers. *Sci. Adv.* **2022**, *8*, No. eabo4021.
(26) Benz, F.; Schmidt, M. K.; Dreismann, A.; Chikkaraddy, R.; Zhang, Y.; Demetriadou, A.; Carnegie, C.; Ohadi, H.; de Nijs, B.; Esteban, R.; Aizpurua, J.; Baumberg, J. J. Single-Molecule Optomechanics in "Picocavities". *Science* **2016**, *354*, 726−729.
(27) Taguchi, A.; Yu, J.; Verma, P.; Kawata, S. Optical Antennas with Multiple Plasmonic Nanoparticles for Tip-Enhanced Raman Microscopy. *Nanoscale* **2015**, *7*, 17424−17433.
(28) Lee, N.; Hartschuh, R. D.; Mehtani, D.; Kisliuk, A.; Maguire, J. F.; Green, M.; Foster, M. D.; Sokolov, A. P. High Contrast Scanning Nano-Raman Spectroscopy of Silicon. *J. Raman Spectrosc.* **2007**, *38*, 789−796.
(29) Yu, J.; Saito, Y.; Ichimura, T.; Kawata, S.; Verma, P. Far-Field Free Tapping-Mode Tip-Enhanced Raman Microscopy. *Appl. Phys. Lett.* **2013**, *102*, No. 123110.
(30) Hartschuh, A.; Anderson, N.; Novotny, L. Near-Field Raman Spectroscopy Using a Sharp Metal Tip. *J. Microscopy* **2003**, *210*, 234−240.
(31) Hartschuh, A.; Qian, H.; Meixner, A. J.; Anderson, N.; Novotny, L. Nanoscale Optical Imaging of Excitons in Single-Walled Carbon Nanotubes. *Nano Lett.* **2005**, *5*, 2310−2313.
(32) Cai, Z.-F.; Merino, J. P.; Fang, W.; Kumar, N.; Richardson, J. O.; De Feyter, S.; Zenobi, R. Molecular-Level Insights on Reactive Arrangement in On-Surface Photocatalytic Coupling Reactions Using Tip-Enhanced Raman Spectroscopy. *J. Am. Chem. Soc.* **2022**, *144*, 538−546.
(33) Yano, T.; Ichimura, T.; Taguchi, A.; Hayazawa, N.; Verma, P.; Inouye, Y.; Kawata, S. Confinement of Enhanced Field Investigated by Tip-Sample Gap Regulation in Tapping-Mode Tip-Enhanced Raman Microscopy. *Appl. Phys. Lett.* **2007**, *91*, No. 121101.
(34) Mahapatra, S.; Jiang, N. Precise Tracking of Tip-Induced Structural Variation at the Single-Chemical-Bond Limit. *Light Sci. Appl.* **2023**, *12*, 21.
(35) Dong, Z. C.; Zhang, X. L.; Gao, H. Y.; Luo, Y.; Zhang, C.; Chen, L. G.; Zhang, R.; Tao, X.; Zhang, Y.; Yang, J. L.; Hou, J. G. Generation of Molecular Hot Electroluminescence by Resonant Nanocavity Plasmons. *Nat. Photonics* **2010**, *4*, 50−54.
(36) Imada, H.; Miwa, K.; Imai-Imada, M.; Kawahara, S.; Kimura, K.; Kim, Y. Single-Molecule Investigation of Energy Dynamics in a Coupled Plasmon-Exciton System. *Phys. Rev. Lett.* **2017**, *119*, No. 013901.
(37) Yokota, Y.; Hong, M.; Hayazawa, N.; Yang, B.; Kazuma, E.; Kim, Y. Self-Consistent Tip Conditioning for Tip-Enhanced Raman Spectroscopy in an Ambient Environment. *J. Phys. Chem. C* **2020**, *124*, 23243−23252.
(38) Su, W.; Kumar, N.; Dai, N.; Roy, D. Nanoscale Mapping of Intrinsic Defects in Single-Layer Graphene Using Tip-Enhanced Raman Spectroscopy. *Chem. Commun.* **2016**, *52*, 8227−8230.
(39) Miranda, H.; Rabelo, C.; Cançado, L. G.; Vasconcelos, T. L.; Oliveira, B. S.; Schulz, F.; Lange, H.; Reich, S.; Kusch, P.; Jorio, A. Impact of Substrate on Tip-Enhanced Raman Spectroscopy: A Comparison Between Field-Distribution Simulations and Graphene Measurements. *Phys. Rev. Res.* **2020**, *2*, No. 023408.
(40) Yeo, B.-S.; Schmid, T.; Zhang, W.; Zenobi, R. Towards Rapid Nanoscale Chemical Analysis Using Tip-Enhanced Raman Spectroscopy with Ag-Coated Dielectric Tips. *Anal. Bioanal. Chem.* **2007**, *387*, 2655−2662.
(41) Hayazawa, N.; Yano, T.; Kawata, S. Highly Reproducible Tip-Enhanced Raman Scattering Using an Oxidized and Metallized Silicon Cantilever Tip as a Tool for Everyone. *J. Raman Spectrosc.* **2012**, *43*, 1177−1182.
(42) Vasconcelos, T. L.; Archanjo, B. S.; Oliveira, B. S.; Silva, W. F.; Alencar, R. S.; Rabelo, C.; Achete, C. A.; Jorio, A.; Cançado, L. G. Optical Nanoantennas for Tip-Enhanced Raman Spectroscopy. *IEEE J. Sel. Top. Quantum Electron.* **2021**, *27*, No. 4600411.

https://doi.org/10.1021/acs.nanolett.4c06273
Nano Lett. 2025, 25, 3707−3716

(43) Deckert-Gaudig, T.; Kämmer, E.; Deckert, V. Tracking of Nanoscale Structural Variations on a Single Amyloid Fibril with Tip-Enhanced Raman Scattering. *J. Biophoton.* **2012**, *5*, 215−219.
(44) Buccini, L.; Proietti, A.; La Penna, G.-C.; Mancini, C.; Mura, F.; Tacconi, S.; Dini, L.; Rossi, M.; Passeri, D. Toward the Nanoscale Chemical and Physical Probing of Milk-Derived Extracellular Vesicles Using Raman and Tip-Enhanced Raman Spectroscopy. *Nanoscale* **2024**, *16*, 8132−8142.
(45) Pandey, Y.; Abbott, D. F.; Mougel, V.; Kumar, N.; Zenobi, R. Probing the Role of Environmental and Sample Characteristics in Gap Mode Tip-Enhanced Raman Spectroscopy. *Anal. Chem.* **2023**, *95*, 8869−8878.
(46) Emory, S. R.; Jensen, R. A.; Wenda, T.; Han, M. Y.; Nie, S. Re-Examining the Origins of Spectral Blinking in Single-Molecule and Single-Nanoparticle SERS. *Faraday Disc.* **2006**, *132*, 249−259.
(47) Cai, Z.-F.; Käser, T.; Kumar, N.; Zenobi, R. Visualizing On-Surface Decomposition Chemistry at the Nanoscale Using Tip-Enhanced Raman Spectroscopy. *J. Phys. Chem. Lett.* **2022**, *13*, 4864−4870.

https://doi.org/10.1021/acs.nanolett.4c06273
Nano Lett. 2025, 25, 3707−3716